Influence of in-plane bending behaviour on textile composite reinforcement forming

R. Bai, E. Guzman-Maldonado, Ruochen Zheng, J. Colmars

Influence of in-plane bending behaviour on textile composite reinforcement forming

R. Bai[a,b,*], E. Guzman-Maldonado[c], R. Zheng[d], J. Colmars[d,*]

[a] *School of Mechanical Engineering, Northwestern Polytechnical University, Xi'an, 710072, China*
[b] *The Key Laboratory of Aircraft High Performance Assembly, Ministry of Industry and Information Technology, Northwestern Polytechnical University, Xi'an, 710072, China*
[c] *Innovamics, 87 Av. des Frères Perret, St-Fons, 69190, France*
[d] *Univ Lyon, INSA Lyon, CNRS, LaMCoS, UMR5259, 69621, Villeurbanne, France*

Abstract

The deformation of textile composite reinforcement is influenced by its fibrous composition. In-plane bending behaviour is an inherent aspect of textile reinforcement, yet it is frequently overlooked. The paper elucidates the significant influence of in-plane bending behaviour on fibre orientation during forming process and emphasizes the necessity of accounting for in-plane bending virtual work to prevent non-physical deformation mode. To this purpose in-plane bending calculation is implemented into a fibrous shell finite element by using the neighbouring elements method.Numerical spurious mode involving in-plane shear is avoided due to the new approach. Finally, the model is validated by comparing with composite reinforcement draping experiments: fibre orientations and distributions of shear angles are simulated in good agreement with experiments and give better results than the simulations neglecting the in-plane bending behaviour.

Keywords: Fabrics/textiles, Composite forming, Finite element method, In-plane bending, Rotation-free shells, Neighbouring element.

1. Introduction

Composite materials are widely used in different sectors due to their high performance and low weight [1, 2, 3, 4, 5, 6, 7]. The manufacture of textile composites often requires Liquid Composites Moulding (LCM) process or thermoforming of prepregs [8, 9, 10, 11, 12, 13]. In both processes, the preforming process is an important step driven by deformations of textile reinforcement. However, this process is often complex. To avoid time-consuming developments by trial and error, it is necessary to apply manufacture process simulations [14, 15, 16, 17]. Different numerical models have been developed for this purpose. Kinematic models were the first methods developed for the forming simulations [18, 19, 20, 21, 22, 23]; these models are very fast, nevertheless, the mechanical behaviour of materials is not considered. Then, some membrane

*Corresponding author
Email addresses: renzi.bai@nwpu.edu.cn (R. Bai), eduardo.guzman@innovamics.com (E. Guzman-Maldonado), julien.colmars@insa-lyon.fr (J. Colmars)

models have been developed neglecting the out-of-plane bending stiffness of textile reinforcements [24, 25, 26, 27, 28], meanwhile, they consider the in-plane shear and tensile behaviour which are specific to fabric. Although the bending stiffness is relatively low due to the possible slippage between fibres [29, 30], the importance of bending stiffness was highlighted with regard to the simulation of wrinkles during the forming of textile reinforcements [31, 32, 33, 34, 35, 36]. Classical shell approaches were adapted to fibrous material, in which the bending stiffness of textile reinforcement will be overestimated if it is deduced from membrane stiffness and section geometry. To consider this specificity, several approaches have been introduced tailored to this challenge. Laminate shell with several layers of different thicknesses and different membrane stiffness were developed [37, 38, 39, 40]. Hybrid element with a combination of a membrane element and a pure bending element with different Young's modulus were proposed [41, 42, 43, 44, 45]. Stress resultant finite element was also proposed to decouple bending and tension modes [46]. All these methods allow a low out-of-plane bending stiffness together with a large membrane stiffness. However, they are based on artificial assumptions that do not reflect the transverse shear along thickness piloted by the quasi-inextensibility of fibre and possible slippage between fibres [47, 48, 49, 50]. In this case, classical shell theory (Kirchhoff, Mindlin) fails to predict the correct solution [51, 52, 53]. The so-called fibrous shell based on the quasi-inextensibility of fibre and the possible slippage between fibres is developed to fill this gap [54]. It has shown that this element provides the correct rotation of material normal by applying the quasi-inextensibility of the fibres at different positions in the thickness.

The majority of numerical approaches based on finite element separate accordingly the internal virtual work into a tension along fibre direction, an in-plane shear and an out-of-plane bending part [55, 56, 57, 58]. However, in-plane bending deformation mode is often overlooked, this mode is related to the in-plane bent fabrics. The in-plane bending deformation of fibre was first observed during the analyses of in-plane shear test including picture frame test and bias-extension test (BET) [59, 60, 61], in these tests, it is possible to see transition zone of shear angle, i.e., in-plane bent fabric. In-plane bending of fabrics was also observed during forming process and related to the occurrence of yarn buckling [62, 63, 64]. Second gradient methods have been proposed for the modelling of this specific phenomenon during BET [65, 66, 67, 68, 69] and were applied to actual forming [70]. However, the implementation of second gradient methods in finite element codes and the determination of associated material parameters are not direct. The use of a non-local finite element technique called neighbouring element technique has been proposed as alternative to higher gradient mechanics [71]; equivalence between the two approaches was discussed on 2D examples in fibrous media. Pentographic beam and membrane meshes were alternatively used in [72, 73, 74] to take into account both in-plane bending and torsional behavior of the textile. In the context of material failure in continuum media, equivalence between non-local integral approaches and gradient-based approaches has been discussed in the past [75, 76]. More specifically in the context of textile forming the two approaches were shown to be equivalent [77, 71]. Nevertheless, most of these studies focus on describing the transition zones in planar tests like BET.

To the author's knowledge, there are few quantitative analyses of this deformation mode and its influences on textile reinforcement forming and yet this point is important since it will influence fibre orientation and distribution during draping. The objective of this article is to highlight the importance of in-plane bending behaviour for textile

reinforcement forming and the specific role of in-plane bending in the occurrence of numerical spurious modes (Section 2). The development of a macroscopic 3D numerical model considering the in-plane bending deformation of textile reinforcement is presented (Section 3). The formulation is implemented in the continuum-based shell specific for fibrous material [78], the calculation of in-plane bending deformation uses the spatial curve constructed with the positions of neighbour elements. The numerical model is first applied to show the influence of in-plane bending behaviour on numerical spurious mode, then the approach is tested through an elementary virtual pull-out test and validated by comparisons with forming experiments (Section 4). The relevance of this approach is validated by the analyses of fibre directions and in-plane bending curvature both in good agreement with experimental results.

2. The influence and importance of in-plane bending deformation

The influence and importance of in-plane bending behaviour are firstly discussed from the experimental point of view and followed by the discussion of the importance of the in-plane bending virtual work in numerical modelling.

2.1. Experimental analyses

2.1.1. Bias-extension test

In Fig. 1a, a specimen of one-layer twill flax is subjected to a bias-extension test. The dimension of the specimen is 210 mm × 70 mm, one end is clamped, and a displacement of 60 mm is imposed at another end. The BET test is considered as a pure shear test to identify the in-plane shear behaviour of textile reinforcement. However, there exists a transition zone visible on Fig. 1a where fabric has a change of in-plane curvature in this zone, this phenomenon is also founded in [60].

2.1.2. Textile composite reinforcement forming test

Textile composite reinforcement forming tests are carried out. A ZwickRoell universal testing machine is used to impose the displacement of the punch. The die and blank holder are transparent and allow the cameras to capture the deformation of the specimen.

For the hemisphere forming test, a specimen composed of four plies Hexcel G1151® initially oriented at 0°/90° is applied. The material properties of Hexcel G1151 are introduced in Table 1. Punch diameter is 150 mm, and punch displacement is 75 mm. In-plane bent yarns and transition zone with gradual change of shear angles are shown in Fig. 1b. Out-of-plane buckling of the fabric is avoided thanks to the blank holder.

Manufacturer	Fibres	Yarn density	Areal density	Thickness
Hexcel	Carbon 6K	7.5 yarns/cm	630 g/m^2	1.3 mm

Table 1: Hexcel G1151 material properties

Fig. 1c shows a tetrahedron forming test of two layers G1151® with the fibre orientation of 0/90°, and the punch displacement is 90 mm. In-plane bent yarns are observed at different zones, which has an influence on the fibre distribution of deformed textile reinforcement. It should be noted that local buckling and yarn slippage occurs in areas

with significant in-plane curvature (zone 1 and 3), indicating that this deformation mode is an important factor for the occurrence of this type of defect [79, 80, 81]. Zone 2 shows a smooth variation of shear angle, related to the variation of curvature. Consequently, considering the in-plane bending behaviour during textile reinforcement forming study has practical significance.

2.2. Numerical analyses

2.2.1. Fibrous shell without in-plane bending virtual work

Numerical analyses proposed in this section are based on a previously developed fibrous shell approach without in-plane bending virtual work [78] which is embedded in the research software Plasfib [82]. This approach considers the possible slippage between fibres through the thickness without adding the virtual transverse shear work. Transverse shear is deduced by the rotation of material director piloted by the quasi-inextensibility of the fibres at different altitude along thickness (Fig. 2). A brief introduction is given below.

The incremental displacement of any point within an element is interpolated as follows:

$$\begin{aligned}\Delta\mathbf{u}\left(\xi,\eta,\zeta\right) = &\sum_{k=1}^{3} N_k \Delta\mathbf{u}_k \\ &+ \sum_{k=1}^{3} N_k \frac{\zeta}{2} ({}^{i}h_m^k + \Delta h_m^k)(\Delta\alpha_k {}^{i}\mathbf{V}_1^k - \Delta\beta_k {}^{i}\mathbf{V}_2^k) \\ &+ \sum_{k=1}^{3} N_k \frac{\zeta}{2} \Delta h_m^k {}^{i}\mathbf{V}_m^k \,,\end{aligned} \tag{1}$$

where ξ, η, ζ are the material coordinates, $\left(\mathbf{V}_1^k, \mathbf{V}_2^k, \mathbf{V}_m^k\right)$ is a local orthogonal frame defined at each node k where $\mathbf{V}_m^k$ is the unit material director.N_k is the shape function at node k. Δu_k is the incremental displacement at node k, $\Delta\alpha_k$ and $\Delta\beta_k$ are the incremental rotation of material director at node k. h_m^k is the thickness along material director direction.

The internal virtual work of this classical approach is the sum of different virtual works of tension $\delta W_{\text{int}}^{Ten}$, out-of-plane bending $\delta W_{\text{int}}^{Bend}$, in-plane shear $\delta W_{\text{int}}^{Shear}$. The assumption that these mechanical behaviours are decoupled is adopted in the proposed approach; it has been shown that the conventional uncoupled model could be acceptable in predicting the general deformation pattern [83], meanwhile the coupling effect is highlighted when the tensile strain is relatively large [84].

The expression of these three terms of virtual work is shown in Eq. 2-4:

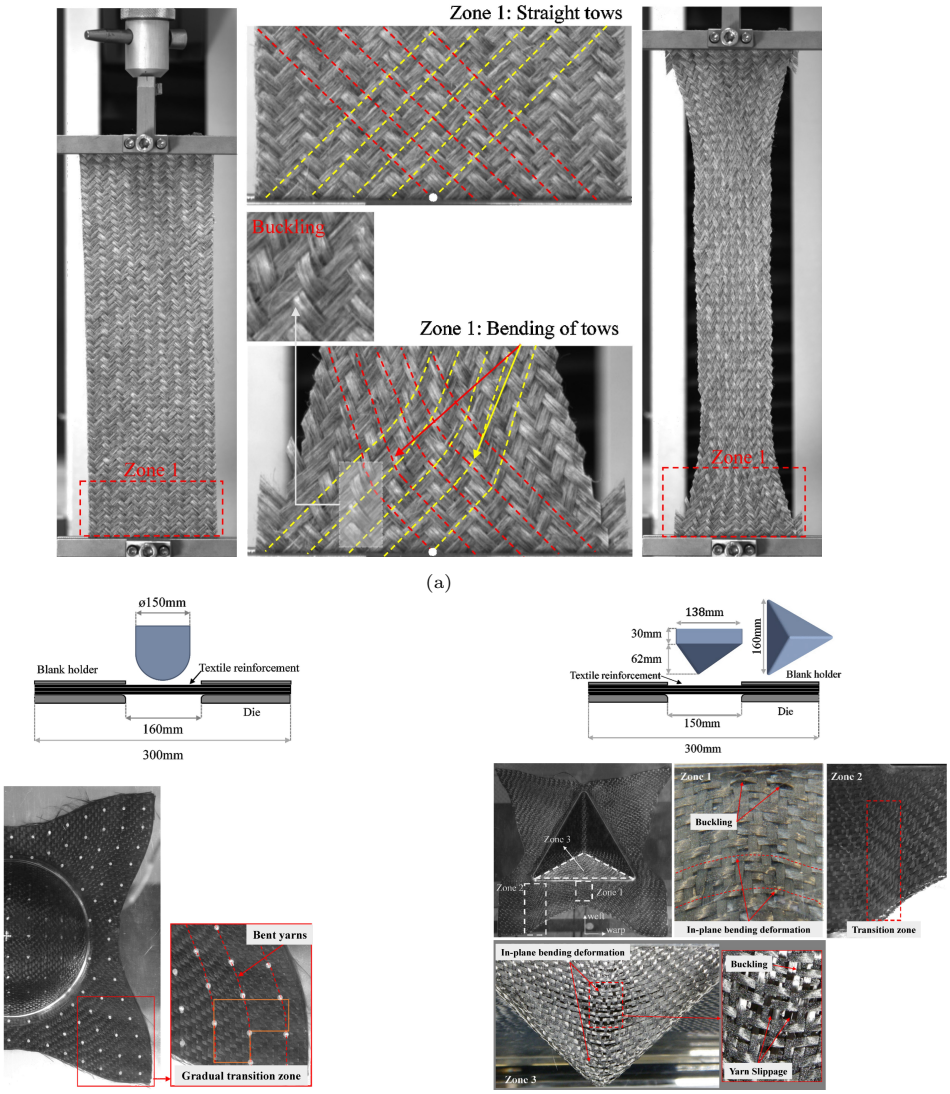

Figure 1: In-plane bending deformations of textile reinforcement. (a) Bias-extension test of Twill Flax. (b) Four layers G1151 hemisphere forming. (c) Two layers G1151 tetrahedron forming.

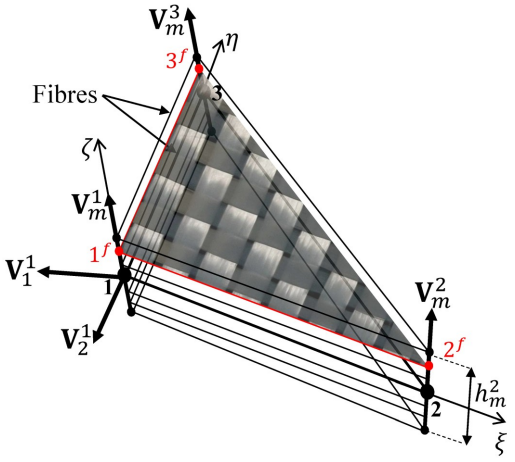

Figure 2: Fibrous shell finite element with 3 nodes where different fibres situated at different altitude along thickness [78].

$$\delta W_{\text{int}}^{Ten} = \sum_{f=1}^{N_{warp}} \int_{L^f} T^{11f}\, \delta\varepsilon_{11}^f\, dL + \sum_{f=1}^{N_{weft}} \int_{L^f} T^{22f}\, \delta\varepsilon_{22}^f\, dL\,, \tag{2}$$

$$\delta W_{\text{int}}^{Bend} = \sum_{f=1}^{N_{warp}} \int_{L^f} M^{11f}\, \delta\chi_{11}^f\, dL + \sum_{f=1}^{N_{weft}} \int_{L^f} M^{22f}\, \delta\chi_{22}^f\, dL\,, \tag{3}$$

$$\delta W_{\text{int}}^{Shear} = \sum_{f=1}^{N_{fibres}} \int_{\Omega} M^{\gamma f}\, \delta\gamma^f\, d\Omega\,. \tag{4}$$

The superscript f indicates the fibre under consideration at different altitudes. N_{warp} and N_{weft} are the number of fibres in warp and weft direction. $\delta\varepsilon_{11}^f$ and $\delta\varepsilon_{22}^f$ are the virtual axial strains in the fibres in warp and weft direction, T^{11f} and T^{22f} are tensions in the fibres in the warp and weft direction. $\delta\chi_{11}^f$ and $\delta\chi_{22}^f$ are the virtual out-of-plane curvatures in the fibres in warp and weft direction, M^{11f} and M^{22f} are out-of-plane bending moment on the warp and weft yarns. $\delta\gamma^f$ is the virtual in-plane shear angle, $M^{\gamma f}$ is the in-plane shear moment. Note that torsional stiffness of the fabric [74] is neglected in our model and has no virtual work associated to it.

All the numerical simulations presented in this article were carried out for the G1151 material. Table 2 presents the tensile, out-of-plane bending and shear properties for the this material which have been identified for this model based on previous works [78]. General material properties are already listed in Table 1. In-plane shear behavior is considered non-linear, while tension and out-of-plane bending stiffnesses are assumed to be linear; this is a simplification since numerous tests have shown that the moment-curvature relationship is non-linear in woven reinforcements [34, 32]. However, to discuss the role of in-plane bending in more detail below, we will keep the hypothesis of a linear bending relationships. The in-plane bending stiffness B_α^{IPB} and the in-plane bending

Tensile	Bending in and out-plane	In-plane shear (IPS)
$T^{\alpha\alpha} = C_\alpha \varepsilon_{\alpha\alpha}$	$M^{\alpha\alpha} = B_\alpha \chi_{\alpha\alpha}$	$M^\gamma = k_1^\gamma \gamma + k_3^\gamma \gamma^3 + k_5^\gamma \gamma^5$
$C_\alpha = 1200$ N·mm^{-1}	$B_\alpha = 6.5$ N·mm	$k_1^\gamma = +4.467e^{-2}$ N·mm
$(\alpha = 1, 2)$	$M_{IPB}^{\alpha\alpha} = B_\alpha^{IPB} \chi_{\alpha\alpha}^{IPB}$	$k_3^\gamma = -4.425e^{-2}$ N·mm
	$B_\alpha^{IPB} = 2B_\alpha$	$k_5^\gamma = +5.292e^{-2}$ N·mm
	$(\alpha = 1, 2)$	

Table 2: Mechanical properties of Hexcel G1151 reinforcement for the proposed numerical model

moment $M_{IPB}^{\alpha\alpha}$ are discussed in details later.

2.2.2. A patch test to highlight in-plane bending contribution

A patch test with four elements is proposed in Fig. 3, the model without in-plane bending work is applied to show its influence. A constant displacement u_y is imposed at nodes *3*, *6*. For nodes *1*, *4*, a displacement $+u_y$ or $-u_y$ is applied respectively to obtain the first configuration with a curved fibre (Case 1) and the second configuration with a straight fibre (Case 2). For both configurations, there is a constant shear angle of 45° for each element, the deformed fibre is represented by $\overline{abc}$ and $\overline{a'bc}$ respectively. The conventional numerical model with in-plane shear virtual work but without in-plane bending virtual work led to the same external work for both configurations, the value of absolute external force at *1-4* side is shown in Fig. 3c. These two different modes cannot be distinguished when neglecting the in-plane bending deformation. This test provides a first justification for the introduction of in-plane bending in the fibrous shell element. Next, we propose a second one.

2.2.3. Non-physical deformation during forming

In the context of forming simulation, spurious deformation mode can be seen when in-plane bending behaviour is not considered. A hemisphere forming simulation is performed without in-plane bending virtual work; nonlinear shear constitutive law is given in Eq. 5, where γ is in-plane shear angle

$$M^s = k_1^\gamma \gamma + k_3^\gamma \gamma^3 + k_5^\gamma \gamma^5 \,. \tag{5}$$

Non-physical zig-zag edges are found at the deformed model (Fig. 4a). For selected elements, the simulation shows unstable evolution of shear angle (Fig. 4b). Indeed, in this area, the fibres are subjected to axial compression and in the absence of in-plane bending stiffness, two solutions are possible for the same in-plane shear field. The fibres will tend to buckle in the plane with this non-physical pattern. The second reason to introduce in-plane bending is to avoid bending spurious mode in forming simulations.

3. Modelling in-plane bending behaviour in textile reinforcement

The specificities of in-plane bending behaviour are discussed in section 3.1 and followed by the development of the numerical model considering in-plane bending deformation.

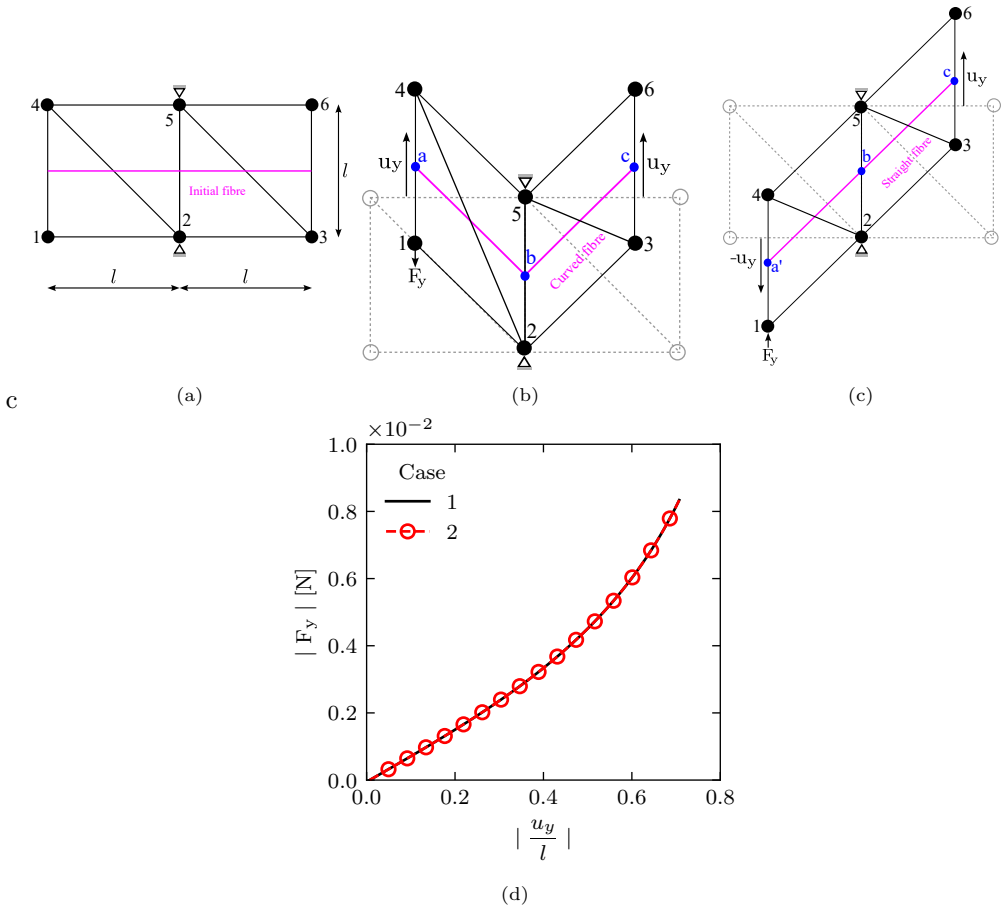

Figure 3: A patch test with two different deformed geometries, (a) Initial mesh, (b) Curved schema (Case 1), (c) Straight schema (Case 2), (d) External force at 1-4 side for cases 1 and 2.

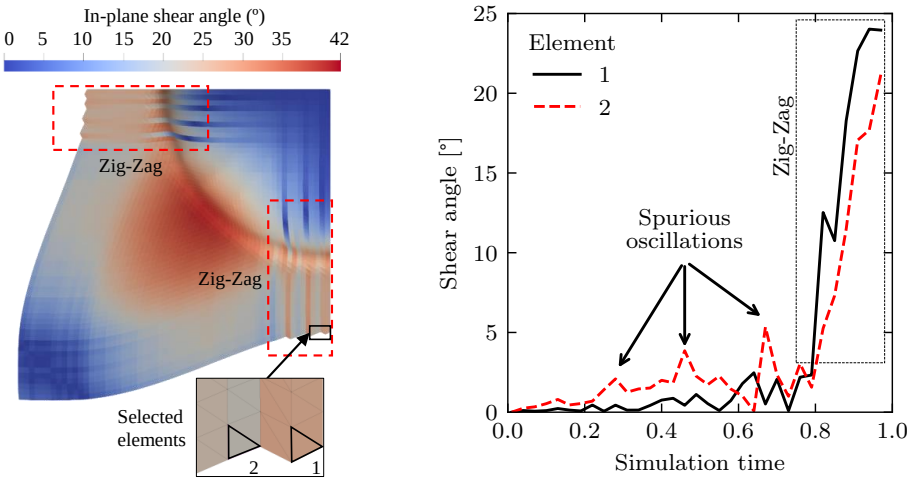

(a) (b)

Figure 4: Forming simulation without in-plane bending virtual work: (a) Deformed geometry with non-physical deformation, (b) Variation of shear angle at selected elements.

3.1. Specificity of textile reinforcement in-plane bending behaviour

According to experimental results, in-plane bending occur in many cases. It is likely to have a non-negligible impact on the final deformed geometry and on the effective reorientation of the fibres during forming. It might be an important factor in the occurrence of defects like buckling (i.e. out-of-plane wrinkling [72]) and yarn slippage. Therefore, the specificity of in-plane bending is studied below following the development of a fibrous shell element considering the in-plane bending behaviour.

First of all, it is important to point out that, as same as out-of-plane bending stiffness, in-plane bending stiffness cannot be deduced directly from the large membrane stiffness of textile reinforcement, because slippage between fibres may occur in and out of the textile reinforcement plane.

In-plane bending deformation causes a relative rotation between warp and weft direction, therefore in-plane bending deformation is kinematically related to the gradient of in-plane shear deformation [71, 85]. Both in-plane shear mode and in-plane bending mode contribute to friction between yarns, consequently, it is difficult to design an experiment to identify separately the in-plane bending constitutive law and the in-plane shear constitutive law. Nevertheless, it is necessary to highlight that these two deformation modes can be decoupled when writing internal virtual work. Similar hypothesis is done in second gradient models where the hyperelastic second gradient strain energy density is supposed to be a function of Cauchy-Green strain gradient only (whereas the first gradient energy is only a function of Cauchy-Green strain) [67, 68, 70]. The in-plane bending behaviour is part of the nature of textile reinforcement: even if there is only one yarn direction (in this case shear angle definition is not straightforward), it is still possible to define in-plane bending field as the gradient of fiber direction. Having two fiber directions means that curvature can be calculated in both directions. In any case the material tends to resist to this deformation, and has a corresponding bending stiffness.

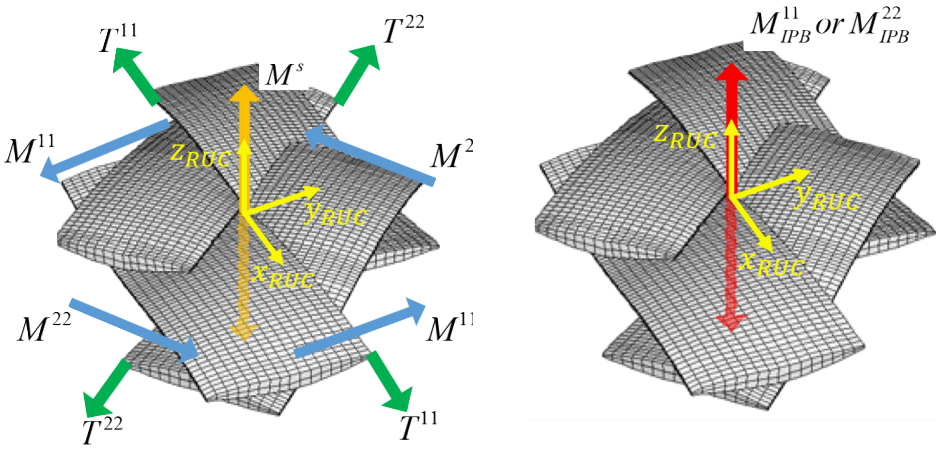

(a) (b)

Figure 5: Loads on a representative unit cell: (a) Tensions, in-plane shear moment and out-of-plane bending moment, (b) In-plane bending moment.

Textile reinforcement can be seen as continuous material made up of woven unit cells (RUC = Representative Unit Cell), thickness of RUC is much smaller than its width. Loads on a RUC are shown in Fig. 5 and are characterized by different load resultants. Three classical behaviours often considered in textile composite are shown in Fig. 5a. In-plane bending loads are shown in Fig. 5b, a local orthogonal frame $(x_{RUC}, y_{RUC}, z_{RUC})$ is defined at the centre of RUC where $x_{RUC} - y_{RUC}$ situate at the plane of RUC, z_{RUC} axe is perpendicular to this plane, M^{11}_{IPB} and M^{22}_{IPB} are in-plane bending (IPB) moment on the warp and weft yarns. The direction of out-of-plane bending moment and in-plane bending moment are different, therefore the role of so-called width and thickness of flexural section is converted for these two cases. This modification of bending section geometry leads to the significant difference between in-plane bending stiffness and out-of-plane bending stiffness.

3.2. Numerical model with in-plane bending virtual work

The numerical model considering the in-plane bending behaviour is developed in the framework of fibrous shell approach [78], where a new term of in-plane bending internal virtual work $\delta W^{IPB}_{\text{int}}$ is added.

$$\delta W_{\text{int}} = \delta W^{Ten}_{\text{int}} + \delta W^{Bend}_{\text{int}} + \delta W^{Shear}_{\text{int}} + \delta W^{IPB}_{\text{int}} \,. \tag{6}$$

The expression of in-plane bending virtual work is shown:

$$\begin{aligned} \delta W^{IPB}_{\text{int}} = & \sum_{f=1}^{N_{warp}} \int_{L^f} \left(M^{11}_{IPB}\right)^f \left(\delta\chi^{IPB}_{11}\right)^f dL \\ & + \sum_{f=1}^{N_{weft}} \int_{L^f} \left(M^{22}_{IPB}\right)^f \left(\delta\chi^{IPB}_{22}\right)^f dL \,, \end{aligned} \tag{7}$$

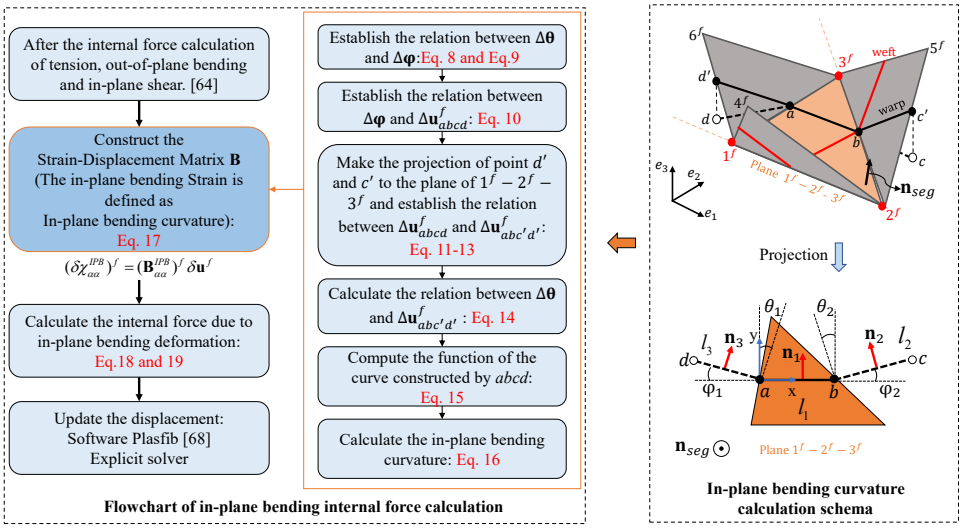

(a) (b)

Figure 6: Calculation of In-plane bending behaviour: (a) Algorithm flowchart, (b) Schema of IPB curvature calculation.

$(\delta\chi_{22}^{IPB})^f$ and $(\delta\chi_{22}^{IPB})^f$ are the virtual in-plane curvatures in warp and weft direction at different fibres, they are calculated from the position of the neighbouring element which is developed for rotation free element [51, 86].

Fig. 6 shows the algorithm flowchart of the developed finite element and the schema of in-plane bending curvature calculation. To avoid numerical locking issues in the triangular element [87], the element edges are aligned with fiber directions; therefore each fibre can pass through the studied element and its two neighbours.

It is possible to define the two endpoints of fibre that pass through each element (Fig. 6b), e.g., four points set (d', a, b, c') are defined at the middle of the element edge and constitute the warp fibre. For the deformed configuration, these four points are possible to situate at different spatial planes, however, the in-plane curvature of fibre is defined in the $1^f-2^f-3^f$ plane, the projection of d' and c' to this plane is therefore calculated and represented by d and c. A local orthogonal co-rotated frame $x-y$ is defined where the point a is the original point, x axis is along the $a-b$ direction, y axis is perpendicular to the x axis and remains in the $1^f-2^f-3^f$ plane. A local third order 2D curve w is fitted using the coordinates of these four points a, b, c, d at local co-rotated frame. This method provides the relation between nodal rotation θ_1, θ_2 and φ_1, φ_2 angles between $ad-ab$, $bc-ab$ at point a and point b:

$$\begin{bmatrix} \theta_1 \\ \theta_2 \end{bmatrix} = \begin{bmatrix} A_{11} & A_{12} \\ A_{21} & A_{22} \end{bmatrix} \begin{bmatrix} \varphi_1 \\ \varphi_2 \end{bmatrix} = \mathbf{A}_{2\times 2} \begin{bmatrix} \varphi_1 \\ \varphi_2 \end{bmatrix}. \tag{8}$$

The values of matrix $\mathbf{A}$ are shown below where l_1, l_2, l_3 are lengths of ab, bc, ad.

$$
\begin{aligned}
A_{11} &= \frac{2}{3}\frac{l_1}{l_1+l_3} + \frac{1}{3}\frac{l_1(l_1+l_2)}{(l_1+l_3)(l_1+l_2+l_3)} \ , \\
A_{12} &= -\frac{1}{3}\frac{l_1 l_3}{(l_1+l_2)(l_1+l_2+l_3)} \, , \\
A_{21} &= -\frac{1}{3}\frac{l_1 l_2}{(l_1+l_3)(l_1+l_2+l_3)} \ , \\
A_{22} &= \frac{2}{3}\frac{l_1}{l_1+l_2} + \frac{1}{3}\frac{l_1(l_1+l_3)}{(l_1+l_2)(l_1+l_2+l_3)} \, .
\end{aligned} \tag{9}
$$

With the incremental displacement of a, b, c, d, the incremental angle can be determined:

$$
\begin{bmatrix} \Delta\varphi_1 \\ \Delta\varphi_2 \end{bmatrix} = \begin{bmatrix} -\frac{(\Delta\mathbf{u}_d^f - \Delta\mathbf{u}_a^f)\cdot\mathbf{n}_3}{l_3} - \frac{(\Delta\mathbf{u}_b^f - \Delta\mathbf{u}_a^f)\cdot\mathbf{n}_1}{l_1} \\ \frac{(\Delta\mathbf{u}_c^f - \Delta\mathbf{u}_b^f)\cdot\mathbf{n}_2}{l_2} - \frac{(\Delta\mathbf{u}_b^f - \Delta\mathbf{u}_a^f)\cdot\mathbf{n}_1}{l_1} \end{bmatrix} = \mathbf{G}_{2\times 12}\Delta\mathbf{u}_{abcd}^f \, , \tag{10}
$$

where $\mathbf{n}_1, \mathbf{n}_2, \mathbf{n}_3$ are normal vectors of segment ab, bc, ad at local frame:

$$
\mathbf{n}_1 = \mathbf{v}_{ba} \times \mathbf{n}_{seg}, \mathbf{n}_2 = \mathbf{v}_{cb} \times \mathbf{n}_{seg}, \mathbf{n}_3 = \mathbf{v}_{ad} \times \mathbf{n}_{seg} \, , \tag{11}
$$

$\Delta\mathbf{u}_{abcd}^f$ is incremental displacement matrix for fibre points a, b, c, d. The displacement of point c and d is the projection of the displacement of point c' and d' at 1^f -2^f -3^f plane.

$$
\begin{aligned}
\Delta\mathbf{u}_c^f &= \Delta\mathbf{u}_{c'}^f - (\Delta\mathbf{u}_{c'}^f \cdot \mathbf{n}_{seg}^f) \cdot \mathbf{n}_{seg}^f \, , \\
\Delta\mathbf{u}_d^f &= \Delta\mathbf{u}_{d'}^f - (\Delta\mathbf{u}_{d'}^f \cdot \mathbf{n}_{seg}^f) \cdot \mathbf{n}_{seg}^f \, .
\end{aligned} \tag{12}
$$

By applying the scalar product with respect to $\mathbf{n}_2, \mathbf{n}_3$, and because $\mathbf{n}_2$ and $\mathbf{n}_3$ are perpendicular to $\mathbf{n}_{seg}^f$, Eq. 12 becomes:

$$
\begin{aligned}
\Delta\mathbf{u}_c^f \cdot \mathbf{n}_2 &= \Delta\mathbf{u}_{c'}^f \cdot \mathbf{n}_2 \, , \\
\Delta\mathbf{u}_d^f \cdot \mathbf{n}_3 &= \Delta\mathbf{u}_{d'}^f \cdot \mathbf{n}_3 \, .
\end{aligned} \tag{13}
$$

Consequently, the incremental nodal rotation $\Delta\theta_1$, $\Delta\theta_2$ is shown below where the $\Delta\mathbf{u}_{abcd}^f$ is replaced directly by $\Delta\mathbf{u}_{abc'd'}^f$:

$$
\Delta\theta_{2\times 1} = \mathbf{A}_{2\times 2}\mathbf{G}_{2\times 12}\Delta\mathbf{u}_{abc'd'}^f \, . \tag{14}
$$

Meanwhile, the curve function can be transformed into the expression below by applying the cubic interpolation:

$$
w = x(1 - \frac{x}{l_1})^2\theta_1 + \frac{x^2}{l_1}(\frac{x}{l_1} - 1)\theta_2 \, . \tag{15}
$$

With an imposed virtual displacement, the virtual curvature of fibre in warp or weft direction at different fibre along thickness is given by:

$$
\begin{aligned}
(\delta\chi^{IPB}_{\alpha\alpha})^f &= \left[\ \tfrac{4}{l_1} - 6\tfrac{x}{{l_1}^2} \quad \tfrac{2}{l_1} - 6\tfrac{x}{l_1}\ \right] \begin{bmatrix} \delta\theta_1 \\ \delta\theta_2 \end{bmatrix} \\
&= \left[\ \tfrac{4}{l_1} - 6\tfrac{x}{{l_1}^2} \quad \tfrac{2}{l_1} - 6\tfrac{x}{l_1}\ \right] \mathbf{AG}\delta\mathbf{u}^f_{abc'd'} \,.
\end{aligned}
\tag{16}
$$

The virtual displacement of a, b, c', d' is interpolated from the displacement of 1^f, 2^f, 3^f, 4^f, 5^f, 6^f, for example, $\delta\mathbf{u}^f_a = \delta\mathbf{u}_{1^f} + \delta\mathbf{u}_{3^f}/2$, therefore, this interpolation is given by $\mathbf{S}_{12\times18}$ matrix and the in-plane bending strain-displacement matrix $(\mathbf{B}^{IPB}_{\alpha\alpha})^f$ is given below.

$$
\begin{aligned}
(\delta\chi^{IPB}_{\alpha\alpha})^f &= \left[\ \tfrac{4}{l_1} - 6\tfrac{x}{{l_1}^2} \quad \tfrac{2}{l_1} - 6\tfrac{x}{l_1}\ \right] \mathbf{AGS}\delta\mathbf{u}^f \\
&= (\mathbf{B}^{IPB}_{\alpha\alpha})^f \delta\mathbf{u}^f \,.
\end{aligned}
\tag{17}
$$

The calculation of in-plane bending internal nodal forces is shown in Eq. 18 where the in-plane bending moment $(M^{\alpha\alpha}_{IPB})^f$ is defined as a function of $(\chi^{IPB}_{\alpha\alpha})^f$. Meanwhile, the membrane force at different fibres in the thickness generates the moments at node k, which contribute to the rotation of material director Eq. 19. The in-plane bending internal load could be obtained by assembling the nodal forces and the nodal moments.

$$
\mathbf{F}^{IPB} = \sum_{f=1}^{n} \Big(\int_L (\mathbf{B}^{IPB}_{11})^{f^T} (M^{11}_{IPB})^f dL + \int_L (\mathbf{B}^{IPB}_{22})^{f^T} (M^{22}_{IPB})^f dL \Big) \,, \tag{18}
$$

$$
\begin{aligned}
M^{IPB}_{\alpha_k} &= \sum_{f=1}^{n} \frac{\zeta h^k_m}{2} ((\mathbf{F}^{IPB}_k)^f \cdot \mathbf{V}^k_1) \,, \\
M^{IPB}_{\beta_k} &= -\sum_{f=1}^{n} \frac{\zeta h^k_m}{2} ((\mathbf{F}^{IPB}_k)^f \cdot \mathbf{V}^k_2) \,.
\end{aligned}
\tag{19}
$$

where ζ and h^k_m are respectively the reference coordinate and the thickness at node k along the material director.

3.3. IPB stiffness value

IPB stiffness is sometimes assumed to be the same as out-of-plane bending stiffness [73, 71]. Although the exact value is not known, Harrison et al. proposed the relation $B^{IPB}_\alpha = 2B_\alpha$ based on inverse method on a BET test [72]. Following the same hypothesis, the IPB stiffness used here is settled as 13 N·mm. The choice of a specific procedure to determine the IPB stiffness must be the subject of more in-depth work.

4. Numerical simulations with in-plane bending energy

Numerical tests are now performed to show the relevance of introducing in-plane bending virtual work. Then, experimental forming tests (hemispherical and tetrahedron) are compared with simulations.

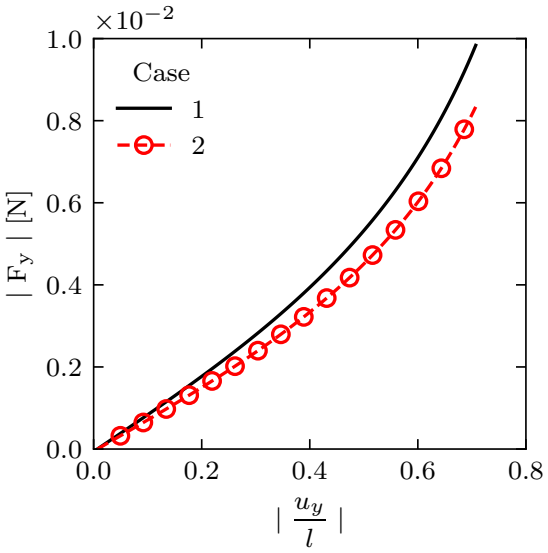

Figure 7: External force at 1-4 side of curved schema (Case 1) and straight schema (Case 2) for simulations considering the in-plane bending virtual work.

4.1. Patch test accounting for the in-plane bending virtual work

The patch test already introduced in section 2.2.2 was conducted without in-plane bending virtual work: in this case the two deformation modes cannot be distinguished numerically. In this section, the same test is performed considering in-plane bending virtual work by using the developed approach. Now the two configurations led to different results: due to the additional term in energy, the force of the bent configuration is larger than the force of the straight configuration (see Fig. 7). In the next section, we show that this addition makes it possible to stabilize in-plane bending spurious modes.

4.2. Stabilization of spurious in-plane bending modes

Forming simulation of section 2.2.3 is now performed with the additional bending energy, all other parameters remain identical. The deformed geometry is shown in Fig. 8a. Stabilization by the bending energy makes it possible to regularize the in-plane shear field. For the selected elements, the effect of stabilization is significant (Fig. 8b).

4.3. Virtual in-plane pull-out test

The pull-out test is initially designed to study yarn buckling, the specific device allows the flexural deformation of fibre (Fig. 9a and Fig. 9b) [63, 80]. For the present work, the kinematic principle of experimental pull-out test will be turned into the virtual in-plane pull-out test, as shown in Fig. 9c, a constant displacement is imposed at the centre of the model, meanwhile, the two ends of the model are free for translation along warp direction. Because of the quasi-inextensibility of fibre, the warp fibre will bear the pull-out deformation at the weft direction.

In-plane bending (IPB) curvature and in-plane shear (IPS) angle are compared between two simulations with and without IPB stiffness, the deformed geometries are shown

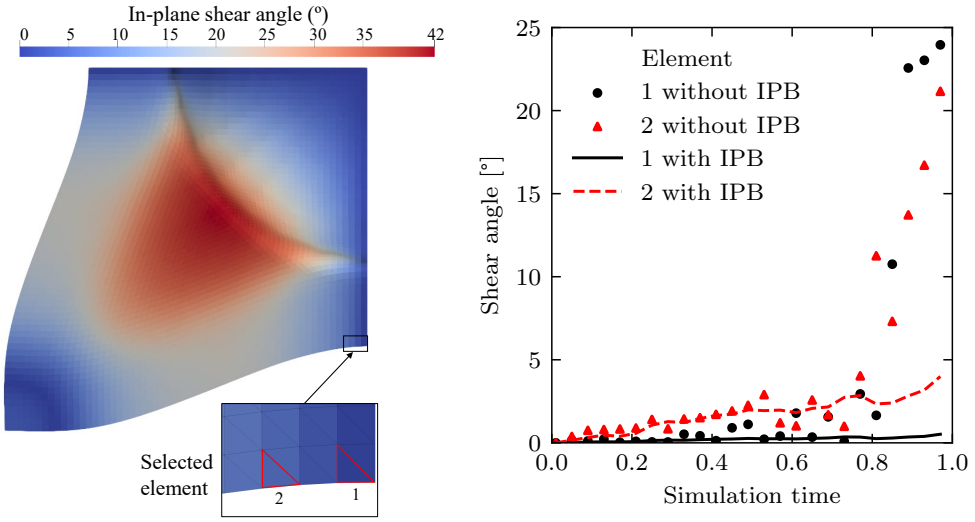

(a) (b)

Figure 8: Forming simulation with in-plane bending virtual: (a)Deformed geometry (c) Shear angle comparison without in-plane bending at selected elements

in Fig. 10. Without IPB stiffness, the displayed IPB curvature is very large at the centre of model, other part remains straight along warp direction ($\chi_{11}^{IPB} = 0$) with a nearly constant shear angle field. This result is not consistent with experimental deformed geometry and is not physical. The deformed model considering IPB virtual work shows a smoother curved edge which corresponds with the experiment, meanwhile, gradual variation of IPB curvature is obtained. The evolution of IPB curvature and IPS angle along the A-B-C path is shown in Fig. 10c, the negative and positive shear angle is distinguished, and curves show that the IPB curvature occurs in shear gradient zones for both two test conditions. Consequently, considering the IPB stiffness provides a realistic deformation with a reasonable distribution of IPB curvature and IPS angles.

4.4. Reinforcement forming: comparison between experiments and simulations

To confirm the importance of in-plane bending (IPB) behaviour and the benefit of the developed approach for textile reinforcement forming, a hemisphere forming test and a tetrahedron forming test are carried out on four plies parallel Hexcel G1151® reinforcement and two plies parallel G1151® reinforcement respectively. Details on forming experiments are presented in section 2.1.

4.4.1. Hemispherical forming

Knowing that the fibres are oriented in single warp and weft directions, the hemisphere forming is modelled by the proposed shell approach using only one element in the thickness; this methodology was validated in [78]. The deformed geometry of the simulation considering the IPB virtual work is compared with the simulation without IPB virtual work (Fig. 11a and b), the edge of shear angles transition zone in Fig. 11a is smoother than that of Fig. 11b.

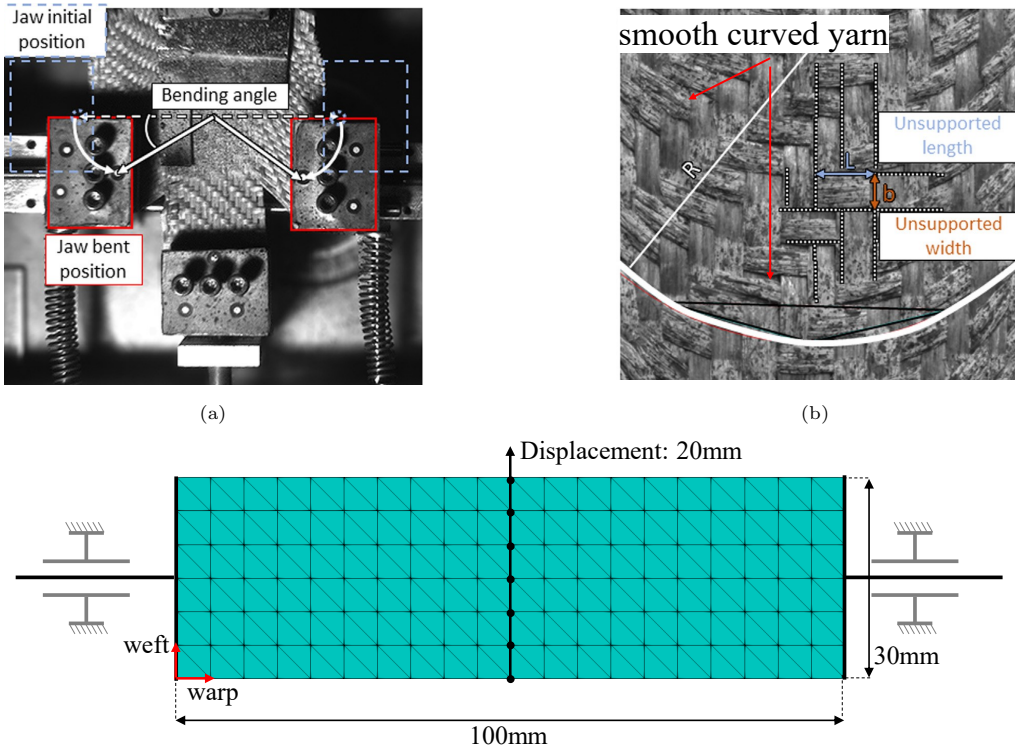

(a) (b)

(c)

Figure 9: Pull-out test: (a) Experiment setup, (b) Bent fabric [80], (c) Simulation schema.

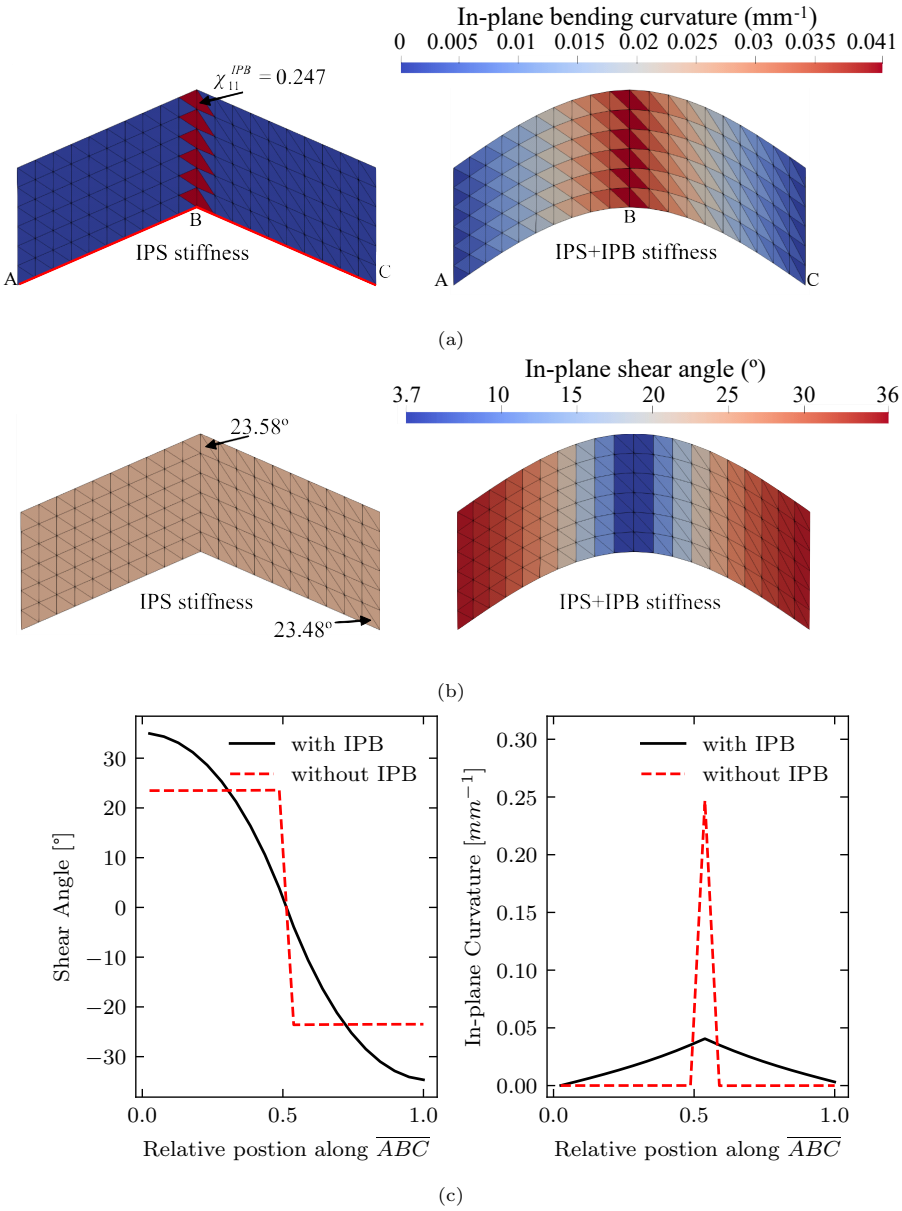

Figure 10: Virtual pull-out test: (a) In-plane bending curvature along warp direction, (b) In-plane shear angle, (c) Shear angle and in-plane bending curvature along $\overline{ABC}$.

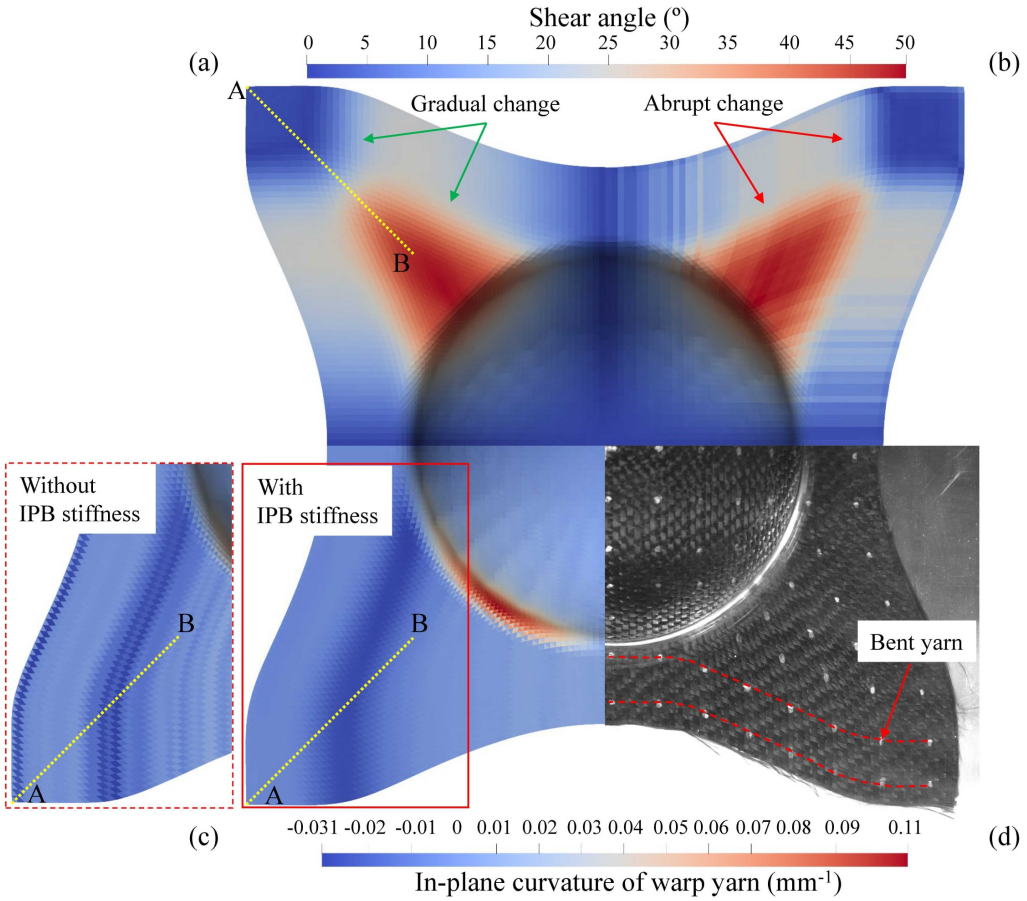

Figure 11: Hemispherical forming of a textile reinforcement at 0/90°. In-plane shear angle: (a) Simulation with IPB stiffness, (b) Simulation without IPB stiffness. In-plane bending curvature along warp direction: (c) Comparison between simulations with IPB stiffness and without IPB stiffness, (d) Experiment.

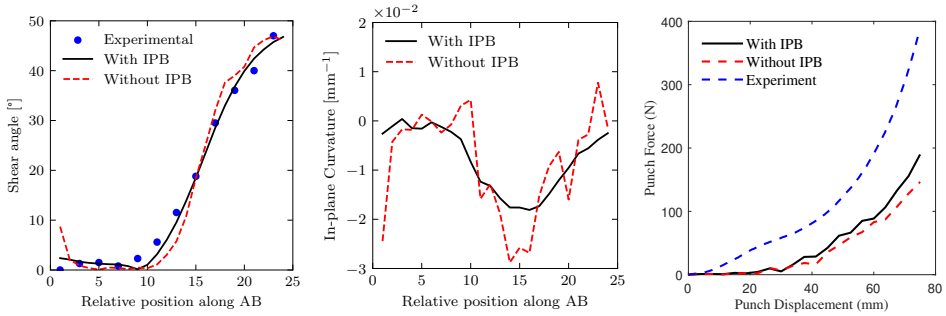

Figure 12: (a) Shear angles along line A-B of Figure 11: Simulations vs Experiment. (b) In-plane bending curvature of warp yarn along A-B: simulation with (black) and without (red) IPB virtual work. (c) Punch force: simulation with (black) and without (red) IPB virtual work vs experiment (blue).

Then, a path A-B is defined at the diagonal direction of the model. The variations of shear angle along A-B for these two simulations and the experiment are shown in Fig. 12a. The maximum difference between numerical results at the same position reaches 4.6°. The model with IPB virtual work shows a gradual variation of shear angles which is closer to the experimental curve (Fig. 12a). The IPB curvature comparison between numerical simulations and experiment is shown in Fig. 11c and d. The variation of IPB curvature along A-B path is shown in Fig. 12b: the simulation with IPB virtual work shows a smooth variation of IPB curvature which is not the case when neglecting the IPB virtual work. Finally, the punch force applied to the reinforcement model is also plotted for the two simulations and the experiment (Fig. 12c). Although the punch force is slightly higher when considering IPB virtual work, the trend of the two curves remains similar, and small differences can be observed in the results. The two simulations have the same trend as the experimental result, although with a significant difference in amplitude. It should be noted on this subject that no friction energy between layers is taken into account in the model; it is very likely that this is the cause of this discrepancy.

4.4.2. Tetrahedron forming

The tetrahedral geometry requires a strongly double-curved deformed shape [88, 89, 90], therefore the modelling of tetrahedron forming is with great interest. Fig. 13 shows the comparison between simulations with and without IPB virtual work.

Fig. 13 a shows the comparison from the shear angle perspective: the simulation with IPB stiffness taken into account gives a more realistic maximum shear angle (61°), compared to the experimental results (59°), than the simulation without IPB virtual (75°) at the same position. Fig. 13b and c present the comparison in terms of curvature in warp and weft direction. The same smoothing effect present on the previous simulations is observed here on the curvatures, leading to significant differences between simulation with and without IPB.

Fig. 14 provides zoom-in view of zone A (defined in Figure 13b). This zoom view makes it possible to more finely compare the changes in orientation of the fibres (Fig. 14a). It is clear that neglecting IPB lead to abrupt changes in fibre direction and non-physical

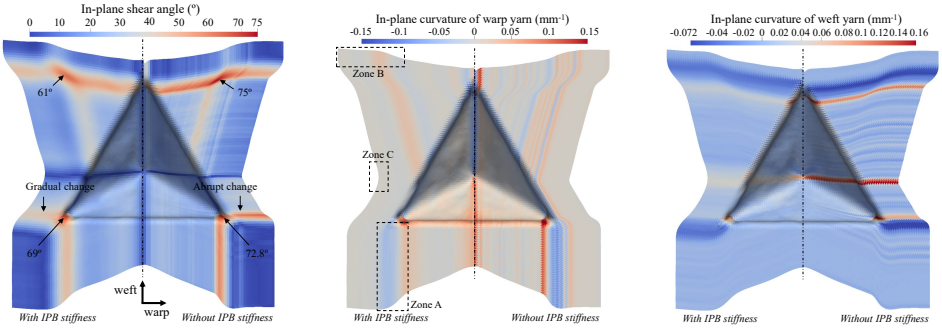

(a) (b) (c)

Figure 13: Simulation of tetrahedron forming of a textile reinforcement at 0/90° (Left: with IPB stiffness, right: without IPB stiffness): (a) In-plane shear angle, (b) In-plane bending curvature along warp direction, (c) In-plane bending curvature along weft direction.

curvatures (Fig. 14b), while results of simulations with IPB stiffness are in excellent agreement with experimental results (Fig. 14c).

More details are provided in Fig. 15a-c (zone B) and Fig. 15d-f (zone C), where the contour is shown in details. Once again, the results considering the IPB virtual work show smoother variations of fibre orientation, and they are in better agreement with experimental results. Edges of Fig. 15c/d are already much better that Fig. 15b/e, but could probably be further improved by a better choice of in-plane bending properties.

5. Conclusion

This work brings various elements showing that it is necessary to take into account the in-plane bending behaviour of fibrous reinforcements during forming analysis. Firstly because it is a part of the nature of textile composite reinforcement, and consequently it has a significant influence on the reorientation of fibre after draping, which was demonstrated numerically. Moreover taking into consideration the in-plane bending virtual work allows the stabilisation of the numerical spurious mode involving in-plane shear. Yet, this behaviour has been so far neglected in most forming simulation approaches.

The fibrous shell approach based on the specific mechanical behavior of textile reinforcement was enhanced considering the in-plane bending curvature with the help of neighbour elements method. The proposed approach has been validated using textile reinforcement forming tests. It has been shown that the prediction of fiber orientation, together with the transition zone of shear angle, are in good agreement with experiments when in-plane bending energy is considered, wheareas neglecting it led to less accurate results.

However, some limitations of this model can be discussed. The hypothesis of decoupling in-plane bending from the other deformation modes should be investigated in future work. Even if the modes are energetically decoupled in virtual work theorem, it is however difficult to show this deformation mode independently of the in-plane shear mode. That is why a direct identification of in-plane bending properties is still a challenging task. The characterization of in-plane bending behaviour need to be addressed

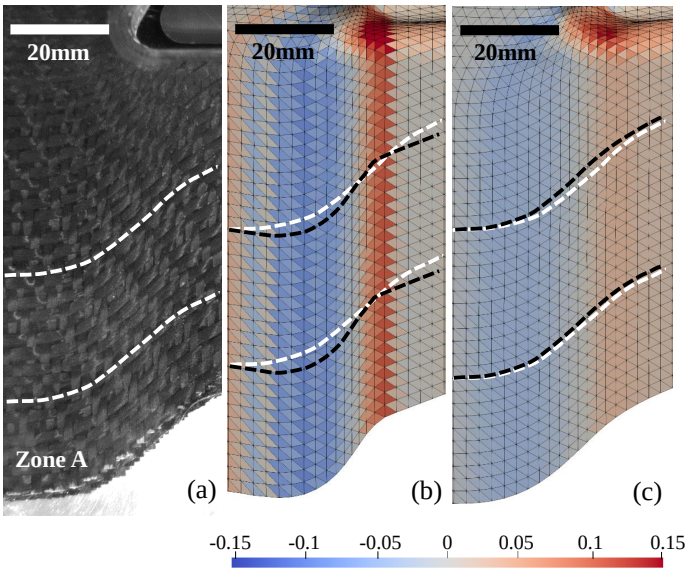

Figure 14: Fibre orientation at zone A (Fig.13b) after deformation: (a) Experiment, (b) Simulation without IPB stiffness, (c) Simulation with IPB stiffness. Experimental and numerical fibre direction are highlighted by white and black dotted line respectively. Coloured field in numerical results show the in-plane curvature of warp yarns, in mm^{-1}.

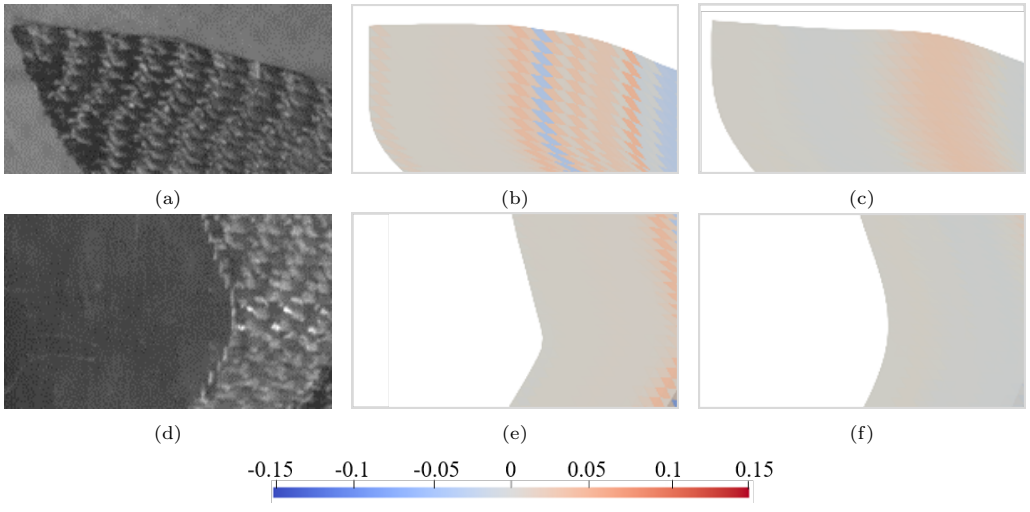

Figure 15: Deformed edges at zones B and C (Fig.13b): (a) (d) Experiment, (b) (e) Simulation without IPB stiffness, (c) (f) Simulation with IPB stiffness. Colorbar shows in-plane curvature of warp yarns, in mm^{-1}.

in future work.

Acknowledgement

The work was supported by the *National Natural Science Foundation of China* [grant number 12302191] and by the Fundamental Research Funds for the Central Universities [grant number D5000220522] and by the French Agence *Nationale de la Recherche* (ANR) [grant N°ANR-18-CE06-0011-04 AMOC].

References

[1] P. Middendorf, C. Metzner, 18 - Aerospace applications of non-crimp fabric composites, in: S. V. Lomov (Ed.), Non-Crimp Fabric Composites, Woodhead Publishing, 2011, pp. 441–449e. doi:10.1533/9780857092533.4.441.

[2] C. Meola, Infrared Thermography in the Evaluation of Aerospace Composite Materials: Non-destructive Evaluation with Infrared Thermography, Woodhead Publishing in Materials, Elsevier, Cambridge, 2015.

[3] H. Towsyfyan, A. Biguri, R. Boardman, T. Blumensath, Successes and challenges in non-destructive testing of aircraft composite structures, Chinese Journal of Aeronautics 33 (3) (2020) 771–791. doi:10.1016/j.cja.2019.09.017.

[4] N. Budwal, K. Kasper, J. Goering, C. Ward, Flexible low-cost tooling solutions for a one-shot resin infusion of a 3d woven and multi-textile preform, Procedia Manufacturing 51 (2020) 856–863. doi:10.1016/j.promfg.2020.10.120.

[5] I. Kimpara, Use of advanced composite materials in marine vehicles, Marine Structures 4 (2) (1991) 117–127. doi:https://doi.org/10.1016/0951-8339(91)90016-5.

[6] P. Feraboli, A. Masini, Development of carbon/epoxy structural components for a high performance vehicle, Composites Part B: Engineering 35 (4) (2004) 323–330. doi:https://doi.org/10.1016/j.compositesb.2003.11.010.

[7] F. Dumont, C. Weimer, D. Soulat, J. Launay, S. Chatel, M. Serge, Composites preforms simulations for helicopters parts, International Journal of Material Forming 1 (2008) 847–850. doi:10.1007/s12289-008-0268-9.

[8] M. Deléglise, P. Le Grognec, C. Binetruy, P. Krawczak, B. Claude, Modeling of high speed RTM injection with highly reactive resin with on-line mixing, Composites Part A: Applied Science and Manufacturing 42 (10) (2011) 1390–1397. doi:10.1016/j.compositesa.2011.06.002.

[9] E. Guzman-Maldonado, N. Hamila, P. Boisse, J. Bikard, Thermomechanical analysis, modelling and simulation of the forming of pre-impregnated thermoplastics composites, Composites Part A: Applied Science and Manufacturing 78 (2015) 211–222. doi:10.1016/j.compositesa.2015.08.017.

[10] H. Xiong, E. Guzman Maldonado, N. Hamila, P. Boisse, A prismatic solid-shell finite element based on a DKT approach with efficient calculation of through the thickness deformation, Finite Elements in Analysis and Design 151 (2018) 18–33. doi:10.1016/j.finel.2018.08.003.

[11] E. Witten, V. Mathes, The market for glass fibre reinforced plastics (GRP) in 2020, AVK: Berlin, Germany (2020).

[12] T. Schmidt, D. May, M. Duhovic, A. Widera, M. Hümbert, P. Mitschang, A combined experimental–numerical approach for permeability characterization of engineering textiles, Polymer Composites 42 (7) (2021) 3363–3379. doi:10.1002/pc.26064.

[13] P. Boisse, R. Akkerman, P. Carlone, L. Kärger, S. V. Lomov, J. A. Sherwood, Advances in composite forming through 25 years of ESAFORM, International Journal of Material Forming 15 (3) (2022) 39. doi:10.1007/s12289-022-01682-8.

[14] P. Bussetta, N. Correia, Numerical forming of continuous fibre reinforced composite material: A review, Composites Part A: Applied Science and Manufacturing 113 (2018) 12–31. doi:10.1016/j.compositesa.2018.07.010.

[15] F. Henning, L. Kärger, D. Dörr, F. J. Schirmaier, J. Seuffert, A. Bernath, Fast processing and continuous simulation of automotive structural composite components, Composites Science and Technology 171 (2019) 261–279. doi:10.1016/j.compscitech.2018.12.007.

[16] B. Liang, P. Boisse, A review of numerical analyses and experimental characterization methods for forming of textile reinforcements, Chinese Journal of Aeronautics 34 (8) (2021) 143–163. doi:10.1016/j.cja.2020.09.027.
[17] Z. Wang, H. Xie, Q. Luo, Q. Li, G. Sun, Optimizaition for formability of plain woven carbon fiber fabrics, International Journal of Mechanical Sciences 197 (2021) 106318. doi:10.1016/j.ijmecsci.2021.106318.
[18] A. C. Long, C. D. Rudd, A Simulation of Reinforcement Deformation during the Production of Preforms for Liquid Moulding Processes, Proceedings of the Institution of Mechanical Engineers, Part B: Journal of Engineering Manufacture 208 (4) (1994) 269–278. doi:10.1243/PIME_PROC_1994_208_088_02.
[19] J. Wang, R. Paton, J. Page, The draping of woven fabric preforms and prepregs for production of polymer composite components, Composites Part A: Applied Science and Manufacturing 30 (6) (1999) 757–765. doi:10.1016/S1359-835X(98)00187-0.
[20] S. Hancock, K. Potter, The use of kinematic drape modelling to inform the hand lay-up of complex composite components using woven reinforcements, Composites Part A: Applied Science and Manufacturing 37 (3) (2006) 413–422. doi:10.1016/j.compositesa.2005.05.044.
[21] C. Mack, H. M. Taylor, 39—the fitting of woven cloth to surfaces, Journal of the Textile Institute Transactions 47 (9) (1956) T477–T488. doi:10.1080/19447027.1956.10750433.
[22] F. L. Heisey, K. D. Haller, Fitting woven fabric to surfaces in three dimensions, The Journal of The Textile Institute 79 (2) (1988) 250–263. doi:10.1080/00405008808659140.
[23] A. Cherouat, H. Borouchaki, L. Giraud-Moreau, Mechanical and geometrical approaches applied to composite fabric forming, International Journal of Material Forming 3 (2010) 1189–1204. doi:10.1007/s12289-010-0692-5.
[24] R. Ten Thije, R. Akkerman, J. Huétink, Large deformation simulation of anisotropic material using an updated Lagrangian finite element method, Computer Methods in Applied Mechanics and Engineering 196 (33-34) (2007) 3141–3150. doi:10.1016/j.cma.2007.02.010.
[25] H. Lin, J. Wang, A. Long, M. Clifford, P. Harrison, Predictive modelling for optimization of textile composite forming, Composites Science and Technology 67 (15) (2007) 3242–3252. doi:10.1016/j.compscitech.2007.03.040.
[26] P. Harrison, R. Gomes, N. Curado-Correia, Press forming a 0/90 cross-ply advanced thermoplastic composite using the double-dome benchmark geometry, Composites Part A: Applied Science and Manufacturing 54 (2013) 56–69. doi:10.1016/j.compositesa.2013.06.014.
[27] S. Chen, L. Harper, A. Endruweit, N. Warrior, Formability optimisation of fabric preforms by controlling material draw-in through in-plane constraints, Composites Part A: Applied Science and Manufacturing 76 (2015) 10–19. doi:10.1016/j.compositesa.2015.05.006.
[28] A. Skordos, C. Monroy Aceves, M. Sutcliffe, A simplified rate dependent model of forming and wrinkling of pre-impregnated woven composites, Composites Part A: Applied Science and Manufacturing 38 (5) (2007) 1318–1330. doi:https://doi.org/10.1016/j.compositesa.2006.11.005.
[29] E. Syerko, S. Comas-Cardona, C. Binetruy, Models of mechanical properties/behavior of dry fibrous materials at various scales in bending and tension: A review, Composites Part A: Applied Science and Manufacturing 43 (8) (2012) 1365–1388. doi:10.1016/j.compositesa.2012.03.012.
[30] P. Boisse, N. Hamila, A. Madeo, The difficulties in modeling the mechanical behavior of textile composite reinforcements with standard continuum mechanics of Cauchy. Some possible remedies, Multiscale Modelling of Fibrous and Textile Materials 154 (2018) 55–65. doi:10.1016/j.ijsolstr.2016.12.019.
[31] B. Liang, P. Chaudet, P. Boisse, Curvature determination in the bending test of continuous fibre reinforcements, Strain 53 (1) (2017) e12213. doi:10.1111/str.12213.
[32] P. Boisse, J. Colmars, N. Hamila, N. Naouar, Q. Steer, Bending and wrinkling of composite fiber preforms and prepregs. A review and new developments in the draping simulations, Composites Part B: Engineering 141 (2018) 234–249. doi:10.1016/j.compositesb.2017.12.061.
[33] L. M. Dangora, C. J. Mitchell, J. A. Sherwood, Predictive model for the detection of out-of-plane defects formed during textile-composite manufacture, Composites Part A: Applied Science and Manufacturing 78 (2015) 102–112. doi:10.1016/j.compositesa.2015.07.011.
[34] F. Yu, S. Chen, L. Harper, N. Warrior, Simulating the effect of fabric bending stiffness on the wrinkling behaviour of biaxial fabrics during preforming, Composites Part A: Applied Science and Manufacturing 143 (2021) 106308. doi:10.1016/j.compositesa.2021.106308.
[35] R. Bai, B. Chen, J. Colmars, P. Boisse, Physics-based evaluation of the drapability of textile composite reinforcements, Composites Part B: Engineering 242 (2022) 110089. doi:10.1016/j.compositesb.2022.110089.

[36] P. Boisse, H. Jin, E. Guzmán Maldonado, Analysis and modeling of wrinkling in composite forming, Journal of Composites Science 5 (2021) 81. doi:10.3390/jcs5030081.
[37] W. R. Yu, M. Zampaloni, F. Pourboghrat, K. Chung, T. J. Kang, Analysis of flexible bending behavior of woven preform using non-orthogonal constitutive equation, Composites Part A: Applied Science and Manufacturing 36 (6) (2005) 839–850. doi:10.1016/j.compositesa.2004.10.026.
[38] O. Döbrich, T. Gereke, O. Diestel, S. Krzywinski, C. Cherif, Decoupling the bending behavior and the membrane properties of finite shell elements for a correct description of the mechanical behavior of textiles with a laminate formulation, Journal of Industrial Textiles 44 (1) (2014) 70–84. doi:10.1177/1528083713477442.
[39] F. Yu, S. Chen, J. Viisainen, M. Sutcliffe, L. Harper, N. Warrior, A macroscale finite element approach for simulating the bending behaviour of biaxial fabrics, Composites Science and Technology 191 (2020) 108078. doi:10.1016/j.compscitech.2020.108078.
[40] M.-G. Han, S.-H. Chang, Draping simulations of carbon/epoxy fabric prepregs using a non-orthogonal constitutive model considering bending behavior, Composites Part A: Applied Science and Manufacturing 148 (2021) 106483. doi:10.1016/j.compositesa.2021.106483.
[41] S. Haanappel, R. Ten Thije, U. Sachs, B. Rietman, R. Akkerman, Formability analyses of uni-directional and textile reinforced thermoplastics, Composites Part A: Applied Science and Manufacturing 56 (2014) 80–92. doi:10.1016/j.compositesa.2013.09.009.
[42] D. Dörr, F. J. Schirmaier, F. Henning, L. Kärger, A viscoelastic approach for modeling bending behavior in finite element forming simulation of continuously fiber reinforced composites, Composites Part A: Applied Science and Manufacturing 94 (2017) 113–123. doi:10.1016/j.compositesa.2016.11.027.
[43] D. Dörr, F. Henning, L. Kärger, Nonlinear hyperviscoelastic modelling of intra-ply deformation behaviour in finite element forming simulation of continuously fibre-reinforced thermoplastics, Composites Part A: Applied Science and Manufacturing 109 (2018) 585–596. doi:10.1016/j.compositesa.2018.03.037.
[44] A. J. Thompson, J. P.-H. Belnoue, S. R. Hallett, Modelling defect formation in textiles during the double diaphragm forming process, Composites Part B: Engineering 202 (2020) 108357. doi:10.1016/j.compositesb.2020.108357.
[45] A. J. Thompson, J. R. McFarlane, J. P.-H. Belnoue, S. R. Hallett, Numerical modelling of compaction induced defects in thick 2D textile composites, Materials & Design 196 (2020) 109088. doi:10.1016/j.matdes.2020.109088.
[46] B. Chen, J. Colmars, N. Naouar, P. Boisse, A hypoelastic stress resultant shell approach for simulations of textile composite reinforcement forming, Composites Part A: Applied Science and Manufacturing 149 (2021) 106558. doi:10.1016/j.compositesa.2021.106558.
[47] M. Mei, Y. He, X. Yang, K. Wei, Analysis and experiment of deformation and draping characteristics in hemisphere preforming for plain woven fabrics, International Journal of Solids and Structures 222–223 (2021) 111039. doi:10.1016/j.ijsolstr.2021.111039.
[48] W. Jiao, L. Chen, J. Xie, Z. Yang, Z. Guo, Deformation mechanisms of 3D LTL woven preforms in hemisphere forming tests, Composite Structures 283 (2022) 115156. doi:10.1016/j.compstruct.2021.115156.
[49] J. Xie, Z. Guo, M. Shao, W. Zhu, W. Jiao, Z. Yang, L. Chen, Mechanics of textiles used as composite preforms: A review, Composite Structures 304 (2023) 116401. doi:10.1016/j.compstruct.2022.116401.
[50] Z. Yang, Y. Jiao, W. Zhu, J. Xie, W. Jiao, L. Chen, Experimental and numerical investigation of inter-ply shear behavior of 3D woven preform, Composite Structures 304 (2023) 116480. doi:10.1016/j.compstruct.2022.116480.
[51] B. Liang, J. Colmars, P. Boisse, A shell formulation for fibrous reinforcement forming simulations, Composites Part A: Applied Science and Manufacturing 100 (2017) 81–96. doi:10.1016/j.compositesa.2017.04.024.
[52] P. Boisse, R. Bai, J. Colmars, N. Hamila, B. Liang, A. Madeo, The Need to Use Generalized Continuum Mechanics to Model 3D Textile Composite Forming, Applied Composite Materials 25 (4) (2018) 761–771. doi:10.1007/s10443-018-9719-8.
[53] B. Chen, J. Colmars, R. Bai, N. Naouar, P. Boisse, Kinematic modeling of transverse shear in textile composite reinforcements forming, International Journal of Mechanical Sciences 245 (2023) 108129. doi:10.1016/j.ijmecsci.2023.108129.
[54] R. Bai, J. Colmars, N. Naouar, P. Boisse, A specific 3D shell approach for textile composite reinforcements under large deformation, Composites Part A: Applied Science and Manufacturing 139 (2020) 106135. doi:10.1016/j.compositesa.2020.106135.

[55] N. Hamila, P. Boisse, F. Sabourin, M. Brunet, A semi-discrete shell finite element for textile composite reinforcement forming simulation, International Journal for Numerical Methods in Engineering 79 (12) (2009) 1443–1466. doi:10.1002/nme.2625.

[56] P. Boisse, N. Hamila, E. Vidal-Sallé, F. Dumont, Simulation of wrinkling during textile composite reinforcement forming. Influence of tensile, in-plane shear and bending stiffnesses, Composites Science and Technology 71 (5) (2011) 683–692. doi:10.1016/j.compscitech.2011.01.011.

[57] P. Wang, N. Hamila, P. Boisse, Thermoforming simulation of multilayer composites with continuous fibres and thermoplastic matrix, Composites Part B: Engineering 52 (2013) 127–136. doi:10.1016/j.compositesb.2013.03.045.

[58] J. Huang, P. Boisse, N. Hamila, I. Gnaba, D. Soulat, P. Wang, Experimental and numerical analysis of textile composite draping on a square box. influence of the weave pattern, Composite Structures 267 (2021) 113844. doi:https://doi.org/10.1016/j.compstruct.2021.113844.

[59] A. Willems, S. Lomov, I. Verpoest, D. Vandepitte, Optical strain fields in shear and tensile testing of textile reinforcements, Composites Science and Technology 68 (3) (2008) 807–819. doi:10.1016/j.compscitech.2007.08.018.

[60] M. Ferretti, A. Madeo, F. dell'Isola, P. Boisse, Modeling the onset of shear boundary layers in fibrous composite reinforcements by second-gradient theory, Zeitschrift für angewandte Mathematik und Physik 65 (3) (2014) 587–612. doi:10.1007/s00033-013-0347-8.

[61] B. Schäfer, R. ZHENG, N. Naim, L. Kärger, Membrane behavior of uni- and bidirectional non-crimp fabrics in off-axis-tension tests, International Journal of Material Forming 16 (2023). doi:10.1007/s12289-023-01792-x.

[62] S. Allaoui, G. Hivet, D. Soulat, A. Wendling, P. Ouagne, S. Chatel, Experimental preforming of highly double curved shapes with a case corner using an interlock reinforcement, International Journal of Material Forming 7 (2) (2014) 155–165. doi:10.1007/s12289-012-1116-5.

[63] C. Tephany, J. Gillibert, P. Ouagne, G. Hivet, S. Allaoui, D. Soulat, Development of an experimental bench to reproduce the tow buckling defect appearing during the complex shape forming of structural flax based woven composite reinforcements, Composites Part A: Applied Science and Manufacturing 81 (2016) 22–33. doi:10.1016/j.compositesa.2015.10.011.

[64] M. Mei, Y. He, K. Wei, X. Yang, Preforming characteristics and defect mitigation strategies for multi-layered biaxial pillar-stitched non-crimp fabric, International Journal of Solids and Structures 267 (2023) 112150. doi:10.1016/j.ijsolstr.2023.112150.

[65] F. dell'Isola, D. Steigmann, A Two-Dimensional Gradient-Elasticity Theory for Woven Fabrics, Journal of Elasticity 118 (1) (2015) 113–125. doi:10.1007/s10659-014-9478-1.

[66] M. d'Agostino, I. Giorgio, L. Greco, A. Madeo, P. Boisse, Continuum and discrete models for structures including (quasi-) inextensible elasticae with a view to the design and modeling of composite reinforcements, International Journal of Solids and Structures 59 (2015) 1–17. doi:10.1016/j.ijsolstr.2014.12.014.

[67] G. Barbagallo, A. Madeo, F. Morestin, P. Boisse, Modelling the deep drawing of a 3D woven fabric with a second gradient model, Mathematics and Mechanics of Solids 22 (11) (2017) 2165–2179. doi:10.1177/1081286516663999.

[68] M. Cuomo, F. dell'Isola, L. Greco, N. L. Rizzi, First versus second gradient energies for planar sheets with two families of inextensible fibres: Investigation on deformation boundary layers, discontinuities and geometrical instabilities, Composites Part B: Engineering 115 (2017) 423–448. doi:10.1016/j.compositesb.2016.08.043.

[69] A. Madeo, G. Barbagallo, M. V. D'Agostino, P. Boisse, Continuum and discrete models for unbalanced woven fabrics, International Journal of Solids and Structures 94-95 (2016) 263–284. doi:https://doi.org/10.1016/j.ijsolstr.2016.02.005.

[70] G. Barbagallo, M. V. d'Agostino, A. Aivaliotis, A. Daouadji, A. Makradi, G. Giunta, P. Boisse, S. Belouettar, A. Madeo, Model reduction for the forming process of fibrous composites structures via second gradient enriched continuum models, Mechanics of Advanced Materials and Structures 28 (10) (2021) 1061–1072. doi:10.1080/15376494.2019.1629050.

[71] Q. Steer, J. Colmars, N. Naouar, P. Boisse, Modeling and analysis of in-plane bending in fibrous reinforcements with rotation-free shell finite elements., International Journal of Solids and Structures 222–223 (2021) 111014. doi:10.1016/j.ijsolstr.2021.03.001.

[72] P. Harrison, Modelling the forming mechanics of engineering fabrics using a mutually constrained pantographic beam and membrane mesh, Composites Part A: Applied Science and Manufacturing 81 (2016) 145–157. doi:10.1016/j.compositesa.2015.11.005.

[73] P. Harrison, M. F. Alvarez, D. Anderson, Towards comprehensive characterisation and modelling of the forming and wrinkling mechanics of engineering fabrics, Multiscale Modelling of Fibrous and

Textile Materials 154 (2018) 2–18. doi:10.1016/j.ijsolstr.2016.11.008.

[74] P. Harrison, L. F. Gonzalez Camacho, Deep draw induced wrinkling of engineering fabrics, International Journal of Solids and Structures 212 (2021) 220–236. doi:https://doi.org/10.1016/j.ijsolstr.2020.12.003.
URL https://www.sciencedirect.com/science/article/pii/S0020768320304765

[75] R. Peerlings, M. Geers, R. de Borst, W. Brekelmans, A critical comparison of nonlocal and gradient-enhanced softening continua, International Journal of Solids and Structures 38 (44) (2001) 7723–7746. doi:10.1016/S0020-7683(01)00087-7.

[76] Z. P. Bažant, M. Jirásek, Nonlocal Integral Formulations of Plasticity and Damage: Survey of Progress, Journal of Engineering Mechanics 128 (11) (2002) 1119–1149. doi:10.1061/(ASCE)0733-9399(2002)128:11(1119).

[77] I. Giorgio, P. Harrison, F. dell'Isola, J. Alsayednoor, E. Turco, Wrinkling in engineering fabrics: a comparison between two different comprehensive modelling approaches, Proceedings of the Royal Society A: Mathematical, Physical and Engineering Sciences 474 (2216) (2018) 20180063. arXiv:https://royalsocietypublishing.org/doi/pdf/10.1098/rspa.2018.0063, doi:10.1098/rspa.2018.0063.
URL https://royalsocietypublishing.org/doi/abs/10.1098/rspa.2018.0063

[78] R. Bai, J. Colmars, B. Chen, N. Naouar, P. Boisse, The fibrous shell approach for the simulation of composite draping with a relevant orientation of the normals, Composite Structures 285 (2022) 115202. doi:10.1016/j.compstruct.2022.115202.

[79] S. Allaoui, C. Cellard, G. Hivet, Effect of inter-ply sliding on the quality of multilayer interlock dry fabric preforms, Composites Part A: Applied Science and Manufacturing 68 (2015) 336–345. doi:10.1016/j.compositesa.2014.10.017.

[80] M. Salem, E. De Luycker, M. Fazzini, P. Ouagne, Experimental, analytical and numerical investigation to prevent the tow buckling defect during fabric forming, Composites Part A: Applied Science and Manufacturing 125 (2019) 105567. doi:10.1016/j.compositesa.2019.105567.

[81] R. Azzouz, S. Allaoui, R. Moulart, Composite preforming defects: A review and a classification, International Journal of Material Forming 14 (6) (2021) 1259–1278. doi:10.1007/s12289-021-01643-7.

[82] LaMCoS, Software Plasfib, Inter Deposit Certification, Agence pour la Protection des Programmes (2011).

[83] M. Komeili, A. Milani, On effect of shear-tension coupling in forming simulation of woven fabric reinforcements, Composites Part B: Engineering 99 (2016) 17–29. doi:10.1016/j.compositesb.2016.05.004.

[84] M. H. Kashani, A. Hosseini, F. Sassani, F. Ko, A. Milani, Understanding different types of coupling in mechanical behavior of woven fabric reinforcements: A critical review and analysis, Composite Structures 179 (2017) 558–567. doi:10.1016/j.compstruct.2017.06.069.

[85] A. Madeo, M. Ferretti, F. dell'Isola, P. Boisse, Thick fibrous composite reinforcements behave as special second-gradient materials: Three-point bending of 3D interlocks, Zeitschrift für angewandte Mathematik und Physik 66 (4) (2015) 2041–2060. doi:10.1007/s00033-015-0496-z.

[86] J.-M. Battini, A rotation-free corotational plane beam element for non-linear analyses, International Journal for Numerical Methods in Engineering 75 (6) (2008) 672–689. doi:10.1002/nme.2267.

[87] N. Hamila, P. Boisse, Tension locking in finite-element analyses of textile composite reinforcement deformation, Comptes Rendus Mécanique 341 (6) (2013) 508–519. doi:https://doi.org/10.1016/j.crme.2013.03.001.
URL https://www.sciencedirect.com/science/article/pii/S1631072113000697

[88] P. Ouagne, D. Soulat, J. Moothoo, E. Capelle, S. Gueret, Complex shape forming of a flax woven fabric; analysis of the tow buckling and misalignment defect, Composites Part A: Applied Science and Manufacturing 51 (2013) 1–10. doi:10.1016/j.compositesa.2013.03.017.

[89] J. Pazmino, V. Carvelli, S. V. Lomov, Formability of a non-crimp 3D orthogonal weave E-glass composite reinforcement, Composites Part A: Applied Science and Manufacturing 61 (2014) 76–83. doi:10.1016/j.compositesa.2014.02.004.

[90] S. Mathieu, N. Hamila, F. Bouillon, P. Boisse, Enhanced modeling of 3D composite preform deformations taking into account local fiber bending stiffness, Composites Science and Technology 117 (2015) 322–333. doi:10.1016/j.compscitech.2015.07.005.